Available online at www.sciencedirect.com

ScienceDirect

Journal of the European Ceramic Society 34 (2014) 327–336

www.elsevier.com/locate/jeurceramsoc

Reactive sintering process and thermoelectric properties of boron rich boron carbides

Sven Roszeitis *, Bing Feng, Hans-Peter Martin, Alexander Michaelis

Fraunhofer IKTS, Institute for Ceramic Technologies and Systems, Winterbergstraße 28, 01277 Dresden, Germany

Received 19 March 2013; received in revised form 13 August 2013; accepted 15 August 2013
Available online 7 September 2013

Abstract

Dense boron rich boron carbides were reactive sintered by hot pressing at 2050 °C using elementary boron–carbon compositions with carbon contents of 9.1, 11.1, 13.3 and 18.8 at.%. The following material characteristics are presented: relative density, SEM images, EDX, X-ray diffraction and corresponding lattice parameters, Seebeck coefficient, electrical conductivity and thermoelectric power factor. Significant grain growth has been obtained with increasing boron content. A deeper understanding of the boron and carbon reaction and the overall sintering process is gained by thermal and chemical analysis in combination with X-ray diffraction. Additionally a thermal experiment with boron and carbon layers illustrates the solid state diffusion behaviour. The found results of boron carbide properties of this paper correspond with results by other authors. The aim is to correlate technological aspects of sintering procedure with material properties. This should help to improve the thermoelectric efficiency of boron carbide based materials.

Keywords: Reactive sintering; Boron carbide; Lattice parameters; Solid state diffusion; Thermoelectrics

1. Introduction

The use of thermoelectric materials for direct conversion of thermal energy into electrical energy is physically linked with a low efficiency. Additionally critical availability and high costs of conventional thermoelectric semiconductors (tellurides) interfere with an economic use of thermoelectric converters. Boron carbide is known as a high temperature resistant thermoelectric material.[1–3] Werheit et al.[3] did show a ZT of about 0.25 at 1200 K and a thermal stability up to 2000 K. The ZT of boron carbide is expected to increase more from 1200 K up to 2000 K.[3] Theoretically, a high efficiency of the energy conversion can be anticipated for boron carbide at temperatures >1200 K (Eq. (1)). The availability of boron carbides is much better than that of established thermoelectric materials such as tellurides or antimonites. But the low thermoelectric performance for temperatures <1200 K requires some effort in material development before boron carbide becomes a promising candidate for thermoelectrics. A better understanding of the reactive sintering process of commercially available boron and carbon powders can help to raise the thermoelectric properties to a higher level and save cost for material manufacture.

The efficiency of the energy conversion is related to the thermoelectric degree of efficiency known as the thermoelectric figure of merit $ZT = S^2\sigma T/\kappa$ and the Carnot efficiency $\eta_C = (T_h - T_c)/T_h$. The theoretical efficiency η can be calculated according to[4]:

$$\eta = \eta_C \frac{\sqrt{1+ZT}-1}{\sqrt{1+ZT}+T_c/T_h} \quad (1)$$

with the thermoelectric properties: Seebeck coefficient S, electrical conductivity σ, thermal conductivity κ, hot side temperature T_h, cold side temperature T_c and mean temperature T. The power factor $S^2\sigma$ is alternatively used to describe the thermoelectric quality of a material.

While Wood and Emin[1] and Aselage et al.[2] suggest polaron hopping as the predominant conduction mechanism in the boron carbides, Werheit[5,6] describes the electronic transport in the boron carbides as a superposition of band-type and hopping-type conduction. Boron carbide is a good p-type thermoelectric

* Corresponding author. Tel.: +49 351 463 32638; fax: +49 351 463 39611.
E-mail addresses: sven.roszeitis@ikts-extern.fraunhofer.de (S. Roszeitis), bing.feng@ikts.fraunhofer.de (B. Feng), Hans-Peter.Martin@ikts.fraunhofer.de (H.-P. Martin), Alexander.Michaelis@ikts.fraunhofer.de (A. Michaelis).

0955-2219/$ – see front matter © 2013 Elsevier Ltd. All rights reserved.
http://dx.doi.org/10.1016/j.jeurceramsoc.2013.08.013

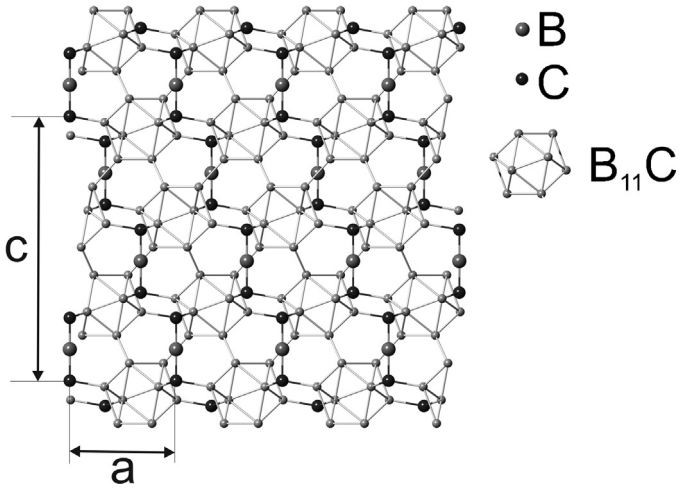

Fig. 1. Section of the hypothetical B_4C structure with the lattice parameters a and c (CBC chains displayed magnified).

material at high temperature. Thermoelectric applications generally need well matching p- and n-type legs. One long standing problem for boron carbide was the lack of a good n-type counterpart. During the last decades, various inventive attempts have been made to obtain a matching n-type boron cluster counterpart.[7] Potential state of the art n-type candidates are homologous rare earth boron carbonitrides[8,9] and yttrium aluminium borides.[10]

Boron carbide exhibits a wide homogeneity range from 8.8 to 18.8 at.% carbon content.[11] The hypothetical B_4C structure (Fig. 1) consists of only $B_{11}C$ icosahedra and C–B–C chains. According to Werheit, the boron carbide structure has no explicit unit cell.[5] The structure consists of a certain mixture of B_{12} and $B_{11}C$ icosahedra and C–B–C, C–B–B and C–vacancy–C chains in dependence of the carbon content.[5] According to the bipolaron model favoured by Aselage and Emin, boron carbides are icosahedral borides that exist as a single phase.[2] Here, boron atoms primarily replace carbon atoms within chains, C–B–C to C–B–B with increasing boron content from $B_{4.3}C$ to $B_{13}C_2$.[2] Further increase of boron content replaces the carbon in the chains C–B–B to B–B–B from $B_{13}C_2$ to $B_{10.5}C$.[2] The bipolaron density peaks at $B_{13}C_2$.[2]

2. Materials and methods

Commercially available amorphous boron and graphite powder were used to produce boron carbide (Table 1).

2.1. Compositions and sintering parameters

Four compositions of amorphous boron and graphite (Table 2) were prepared by ball milling (PM4000, Retsch, Germany) using liquid phase sintered silicon carbide balls, isopropanol and about 0.1 wt.% of an organic dispersant (KV 5151, Zschimmer & Schwarz GmbH & Co KG, Germany).

The mass of the abrasion of the silicon carbide balls reaches about 0.7 wt.% of the starting powder mass. Hence, the abrasion of the silicon carbide balls caused an additional contamination of the compositions with silicon, carbon and small amounts of aluminium (sintering aid of the silicon carbide balls). Every further specimen was sintered from one of these four compositions. The carbon content of initial weight c_C (Table 2) is calculated according to:

$$c_C = \frac{m_{\text{Graphite}} \cdot P_{\text{Graphite}}/M_{\text{Carbon}}}{(m_{\text{Graphite}} \cdot P_{\text{Graphite}}/M_{\text{Carbon}}) + (m_{\text{A.Boron}} \cdot P_{\text{A.Boron}}/M_{\text{Boron}})} \quad (2)$$

Each corresponding powder masse m is multiplied by the powder purity P (Table 1) and divided by the molar mass M. Hence, the carbon content of initial weight relates only to the sum of carbon and boron atoms. The powder impurities and the abrasion of the silicon carbide balls from milling are neglected for this consideration.

The carbon content of the prepared compositions was chosen according to the homogeneity range of the boron carbide phase (8.8–18.8 at.% carbon[11]). 9.1 at.% carbon were chosen instead of 8.8 at.% carbon to avoid residual boron in the sintered compacts with high certainty. Thermal analysis was done with excess carbon (20 at.%).

The Sintering parameters are shown in Table 3. The graphite die was coated by a thin film of boron nitride to impede carbon and boron diffusion between sintering compact and die.

During the sintering process boron and carbon react exothermically to boron carbide:

$$x\text{B} + \text{C} \rightarrow \text{B}_x\text{C} \quad (3)$$

Table 1
Raw material characteristics.

	Amorphous boron	Graphite
Product name	Amorphous Boron Grade 1	Graphit-Pulver Feinst 4
Manufacturer	H.C. Starck, Goslar, Germany	Fuchs Lubritech GmbH, Dohna, Germany
Powder purity[a] (Minimum)	95 wt.%	99.5 wt.%
H_2O soluble[a]	0.2 wt.%	–
H_2O_2 insoluble[a]	1.0 wt.%	–
Moisture[a]	0.5 wt.%	–
O[a]	2.2 wt.%	–
N[a]	0.4 wt.%	–
Mg[a]	0.8 wt.%	–
d_{10}	0.5 μm	1.8 μm
d_{50}	1.5 μm	5.2 μm
d_{90}	4.6 μm	11.2 μm

[a] Originated from data sheet of manufacturer.

Table 2
Amorphous boron—graphite – compositions and their carbon content of the initial weight.

Composition number	Carbon content of the initial weight (at.%)	Stoichiometry
1	9.1	$B_{10}C$
2	11.1	B_8C
3	13.3	$B_{13}C_2$
4	18.8	$B_{4.3}C$
Thermal analysis	20.0	B_4C

Table 3
Sintering parameters.

Sintering temperature (°C)	2050
Sintering technique	Hot pressing
Press model, manufacturer	HPW200, FCT System
Atmosphere	Argon
Pressure (MPa)	50
Heating rate (K/min)	10
Holding time (min)	60
Cool down (K/min)	10

Either the boron carbide formation results directly in the final superstoichiometric boron carbide or a temporary boron–carbon compound is formed which incorporates more boron after the primary formation of boron carbide according to Eq. (4):

$$yB + B_xC \rightarrow B_{x+y}C \quad (4)$$

An experiment was designed to investigate the interactivity of boron and carbon based on diffusion. This experiment was performed by using boron powder as it is used for boron carbide synthesis (Table 1) in combination with graphite disks. The boron powder is filled in a graphite tool which is coated with boron nitride to prevent strong interactions and contains already a graphite disc on the bottom. A second graphite disc is put onto the boron powder so that it is placed between the two discs. The tool is heated up to 2050 °C in the hot press furnace under a pressure of 50 MPa. The heating up rate was 10 K/min. The sample is hold at maximum temperature for 60 min. After cooling down the sample is removed and small specimen of the interlayer B–C together with graphite and boron sections are prepared for FESEM and EDX analysis.

2.2. Geometries and analyses

The powder compositions were sintered to tablets of 30 mm diameter and 7.5 mm height. The tablets were mechanical polished and cut into the geometries, which are required for the different characterisation methods planed (Fig. 2).

The high temperature measurements were performed in inert atmosphere (argon or nitrogen) to avoid oxidation of boron carbide.

In order to study the reaction process of the sample during sintering, thermogravimetric analysis (TG), differential thermal analysis (DTA) and differential thermogravimetric analysis (DTG) were carried out on a powder with 20 at.% carbon content using a Netzsch STA 449 F1 thermal analyser at a temperature up to 1800 °C in Argon.

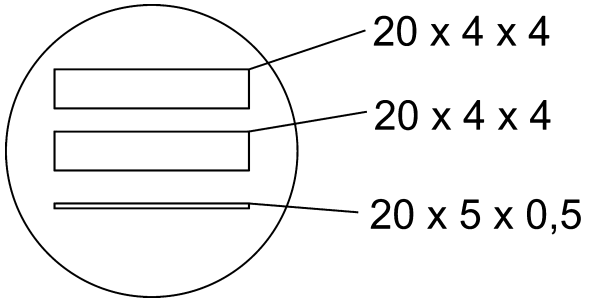

Fig. 2. Location of specimen geometries in a tablet, all dimensions in millimetres.

The composition of the hot pressed sample with 11.1 at.% carbon content of initial weight was determined via chemical analysis by the ESK Ceramics GmbH & Co. KG (Germany). The chemical analysis included an alkaline fusion with titrimetric determination of the boron content. The carbon content was determined by burning under oxygen with an infra-red detector. Oxygen and nitrogen were determined by carrier gas hot extraction. The free carbon content was determined by wet-chemical oxidation with iodine/chromium sulphuric acid at 80 °C and coulometric detection of carbon dioxide. Further elements were determined via DC-ARC-OES.

The microstructure of sintered specimens was characterised by field emission scanning electron microscopy (ULTRA 55, CARL ZEISS, Germany) equipped with an energy dispersive X-ray detector (EDX). Samples for microscopy were prepared from residual parts of sintered pellet (Fig. 2).

The phase analysis was carried out by X-ray diffraction with Cu K_α radiation ($\lambda = 1.54$ Å) (D8 ADVANCE, Bruker AXS) using the plane surface of the mechanical polished tablets.

To determine the lattice parameters of the samples the sintered specimens were milled to powder and mixed with 10 wt.% of silicon as standard reference material. The silicon reflexes were used to correct the Bragg angle. Rietveld analysis was performed using the software TOPAS (Bruker AXS).

The Seebeck coefficient was determined on specimens with the size of 20 mm × 5 mm × 0.5 mm (measuring instrument built by PhysTech, Germany). During the measurement the area of $20 \times 5\ mm^3$ was in direct contact with a two point heater, which provides a defined temperature gradient. The opposite side of the contact face between heater and specimen has two electrical contacts to measure the thermo-voltage induced by the temperature gradient.

The electrical conductivity was determined by the four point probes method in a glass tubular furnace. Specimens with the size of 20 mm × 4 mm × 4 mm were used.

2.3. Relative density

The density of boron carbide depends on its carbon content. The theoretical density ρ_{th} is calculated according to Bouchacourt and Thévenot[12–14]:

$$\rho_{th} = 2.422\ g/cm^3 + 0.0048\ g/cm^3\ c_C/at.\% \quad (5)$$

where c_C is the carbon content of the initial weight (Eq. (2)).

3. Results and discussion

3.1. Thermal analysis

The curves of the thermal analysis of a powder mixture (B + C) with 20 at.% carbon content are shown in Fig. 3. The

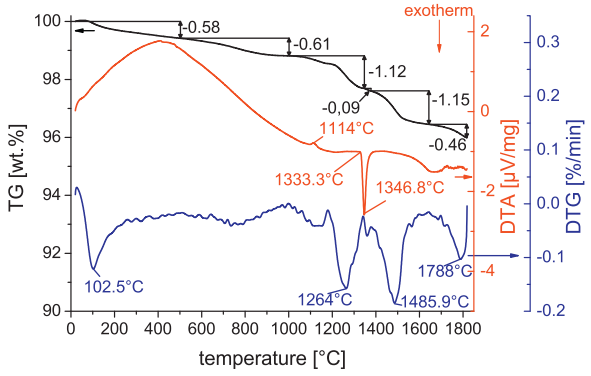

Fig. 3. TGA, DTA and DTG of a composition with 20 at.% carbon content of the initial weight.

DTA curve shows a slight endothermic peak at 1114 °C, which is related to a reaction of oxygen impurities:

$$2B_2O_3\,(l) + 7C\,(s) \rightarrow B_4C\,(s) + 6CO\,(g) \quad (6)$$

Reaction (6) was observed in the work of Sinha et al. during heating up a precursor powder consisting of boron oxide and carbon at a temperature of 1127 °C.[15] In the work of Najafi et al. this reaction (6) was observed at a temperature of 1270 °C in a boron alkoxid precursor system.[16] The different reaction temperatures indicate that the start of this reduction of boron oxide in combination with the oxidation of carbon depends on the chemical situation of starting compounds and elemental distribution. Oxygen impurities are most likely present as B_2O_3 in the amorphous boron powder component (Table 1). An additional formation of B_2O_3 may occur during the previous ball milling of the composition under air atmosphere so that some more oxygen is present than in the original powder (Table 1).

The main exothermic reaction (71.2 kJ/mol[17]) between boron and carbon (Eq. (3)) starts at about 1333.3 °C according to our investigations (Fig. 3). This reaction temperature of about 1333 °C is in good correlation with the XRD observed phase content at 1300 °C (carbon + boron) and 1400 °C (carbon + boron + boron carbide) in the work of Wang et al.[18] The previous oxide reduction may initiate the carbide formation. There is no further thermal effect observed at higher temperatures. But the TG/DTG curves show more mass loss.

The TG curve indicates a mass loss of about 0.58 wt.% up to 500 °C corresponding to the evaporation of moisture and other volatiles of the sample. With increasing temperature the mass loss reached 4 wt.% due to the formation of the gaseous products CO, B_2O_3 (g), B_2O_2 (g) and B_2O (g) or evaporation of impurities (e.g. B_2O_3 (s) → B_2O_3 (g)).

The DTG curve shows four peaks corresponding to the TG change. The fourth peak at 1788 °C is probably an evaporation process of impurities like MgO. Compared to the total mass of the sample the mass loss is insignificant and most probably linked to the impurities of boron and carbon (Table 1). The boron carbide formation (Eq. (3)) is not linked with any mass change.

Table 4
Chemical analysis of sample 11.1 at.% carbon content of initial weight after hot pressing.

Element	Content (at.%)
B	86.33
C (solved in B_xC and SiC)	12.01
O	1.04
Si (from SiC phase)	0.30
N	0.18
Mg	0.05
Al	0.04
C (free)	0.03
Fe	0.008
Ti	0.003
Ca,	0.003
Mn	0.001
Cr	0.0003
Ni	0.0003

3.2. Chemical analysis after hot pressing

Table 4 shows the chemical analysis of the sample with 11.1 at.% carbon content of initial weight after hot pressing. Some of the raw materials impurities (Table 1) did evaporate during sintering, but oxygen, nitrogen and magnesium are still present. In addition small amounts of silicon (grinding balls), aluminium (sintering aid of the grinding balls) and iron impurities (grinding jar) are to be found after hot pressing as result of the powder milling process. There are very small amounts of the further impurities. These impurities are mostly alloy elements of the grinding jar steel.

The determined silicon is part of a silicon carbide phase in the sample (abrasion of the grinding balls). The silicon carbide increases the carbon content of the sample with 0.3 at.% (equivalent to its silicon content, Table 4). The silicon carbide phase is thermodynamically stable during the sintering process, but will not be detected by the following X-ray diffraction analysis of the hot pressed samples (less than 1 vol.%). Therefore, 0.3 at.% of the determined carbon content are most probably associated with the silicon carbide phase. The carbon content referred to the boron carbide phase of 11.7 at.% after sintering is in good correspondence to 11.1 at.% before sintering. The cause of this slight increase of the carbon content is the evaporation of boron oxides (cf. Fig. 3) during the hot pressing process.

Because of the uniform preparation process the other samples with 9.1, 13.3 and 18.8 at.% carbon content of initial weight should include comparable impurities. Their carbon content should show a slight increase after hot pressing, too.

3.3. Diffusion process of boron and carbon during the hot pressing process

A carbon (graphite disc) – boron (amorphous powder) – carbon (graphite disc) – sandwich was hot pressed at 2050 °C (same sintering parameters as the other hot pressed specimens, Table 3) to gain an impression of the diffusion intensity of boron and carbon during hot pressing.

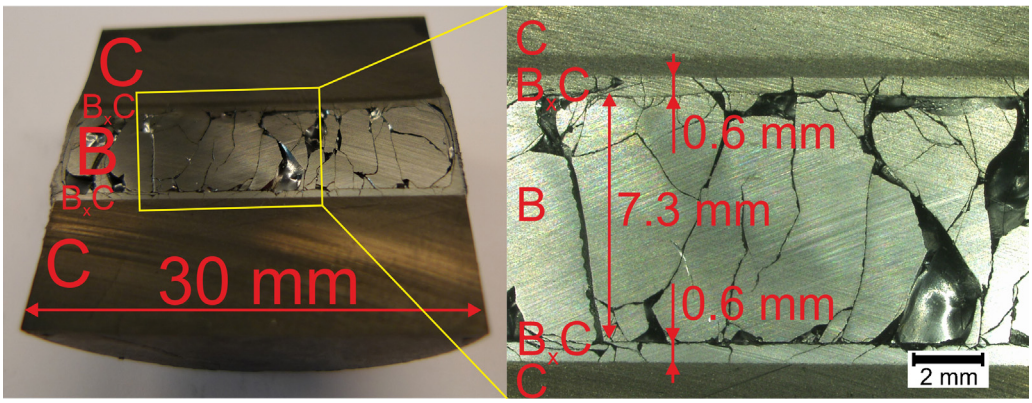

Fig. 4. Cut hot pressed sandwich displaying the formed reaction zone consisting of boron carbide (B_xC) between carbon (C) and boron (B) layer.

After hot pressing the sandwich consisted of three distinguished zones (Fig. 4): carbon (C) – boron carbide (B_xC) – boron (B) and again – boron carbide (B_xC) – carbon (C). The upper reaction zone (C–B_xC–B) is of the same size (about 0.6 mm) as the lower reaction zone (B–B_xC–C) (Fig. 4). Cracks are located all over the boron and boron carbide layers and indicate high thermo-mechanical stress during the cool down. The material breakout in the boron and boron carbide layers was caused by preparation procedure and is not related to the hot pressing process. The upper and lower carbon layer exhibit no cracks or other material defects.

The formation of an upper and lower boron carbide layer in the hot pressing process can be described by the following way with concern to the already reported findings from thermal analysis and XRD:

(1) At the beginning the pressure of the hot press causes flow of the boron powder particles and elastic deformation of the boron powder and the carbon layer. The deformation of boron and carbon enables the compaction of the boron powder.
(2) At about 1333 °C (according to DTA results) the reaction of boron and carbon to boron carbide starts at the upper and lower contact face between boron and carbon. The formed boron carbide layer separates the boron and carbon layers.
(3) The further formation of boron carbide needs diffusion of boron or, respectively, carbon through the boron carbide layer. The formation of additional boron carbide is limited by both diffusion rates.
(4) At about 2040 °C the residual boron layer probably melts. Carbon and boron carbide are still in the solid state. The diffusion of boron and carbon through the boron carbide layer continues.
(5) During cool down the boron solidifies. The shrinkage of the sintered boron powder causes high thermo-mechanical stress, what causes cracks. The overall formation of boron carbide stops beneath a temperature of about 1300 °C.

The boron, carbon and oxygen content of the lower reaction zone was determined by energy dispersive X-ray spectroscopy (Fig. 5) with an absolute error of about one atom per cent and a local blur of about one micrometre, which is the area of excitation of the electron beam. The local blur of about one micrometre should be negligible in comparison to the investigated dimension, which is about 600 μm. The local transition from boron to boron carbide (points 2–4 in Fig. 5b) is sharp. The observed transition is influenced by thermo mechanical induced cracks which are filled with epoxide resin during FESEM preparation of the

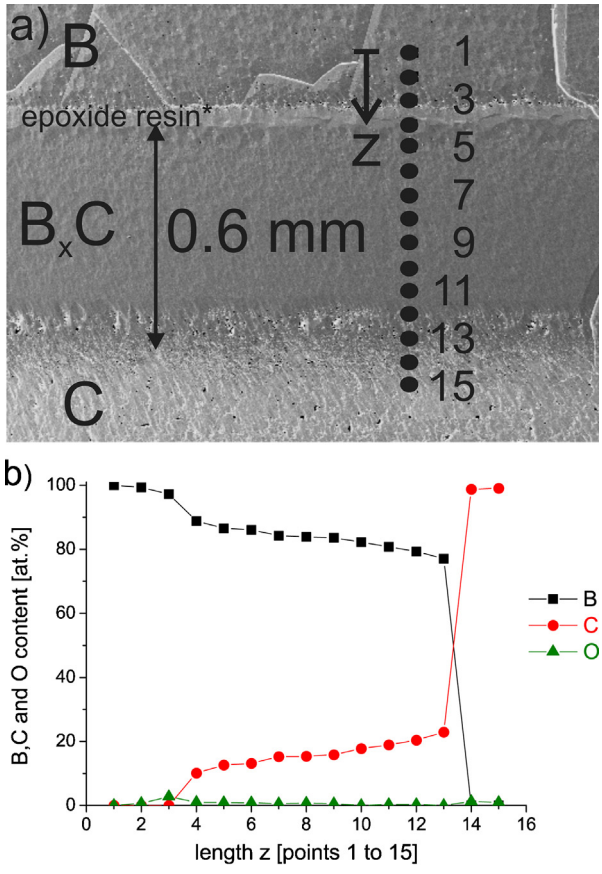

Fig. 5. Lower reaction zone (B – epoxide resin* – B_xC – C) of the hot pressed sandwich (a) FESEM image (b) corresponding energy dispersive X-ray spectroscopy with the elements boron (B), carbon (C) and oxygen (O) * derived from FESEM preparation.

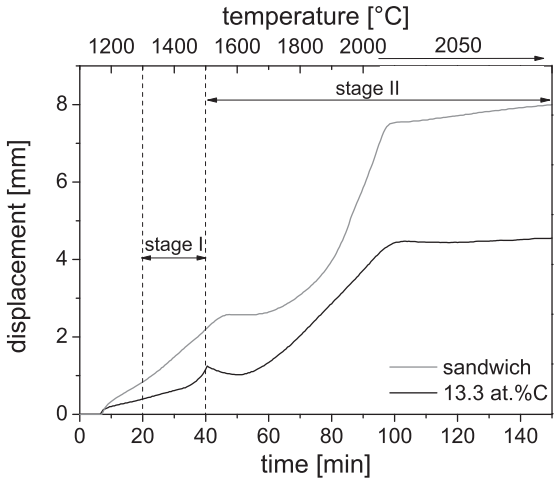

Fig. 6. Displacement in pressing direction during hot pressing of the sandwich and the sample with 13.3 at.% carbon content of the initial weight.

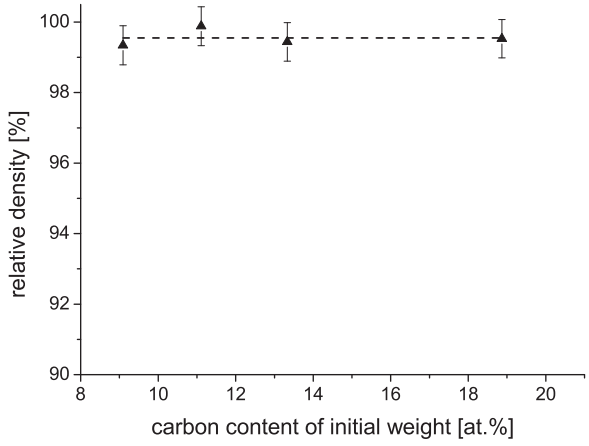

Fig. 7. Relative density in dependence of the carbon content of the initial weight after hot pressing at 2050 °C.

sandwich (points 3–4 in Fig. 5a). The observed oxygen (point 3 in Fig. 5b) is part of the epoxide resin and no component of the original sandwich. The reaction product (boron carbide B_xC) forms an upper and lower layer of 0.6 mm length (Figs. 4 and 5) with a gradual increase of the carbon content in carbon direction from 10 at.% (point 4 in Fig. 5b) to 23 at.% (point 13 in Fig. 5b). The observed carbon content is in the field of the homogeneity range of the boron carbide phase (8.8–18.8 at.% carbon[11]) and the two phase area of boron carbide and carbon (>18.8 at.% carbon[11]). A sharp local transition from boron carbide to carbon is observed (points 13–14 in Fig. 5b) with increasing carbon content.

The two shown boron carbide reaction layers (Fig. 4) are a product of mixing derived by deformation and diffusion. The separation of diffusion effects and deformation effects is impossible by this experimental approach, but the gradual carbon increase in the boron carbide layer (Fig. 5b) is an indication, that the structure of the boron carbide layer is mostly caused by diffusion rather than mixing by deformation.

The information about the diffusion process of boron and the diffusion process of carbon in boron carbide, which are gained by this experiment, are helpful for interpretation of further experiments concerning the B–C derived formation of B_xC. The size of the boron carbide reaction layers of 0.6 mm (Figs. 4 and 5) is about two orders of magnitude larger than the original particle

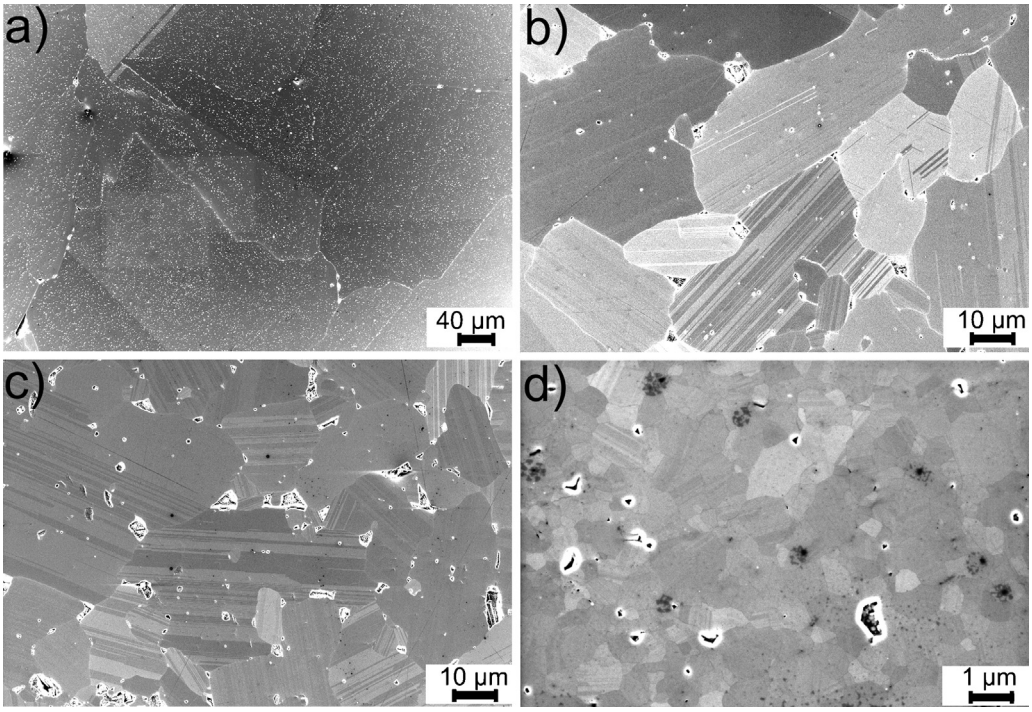

Fig. 8. FESEM images looking parallel to the pressing direction of the samples; carbon content of the initial weight from 9.1 to 18.8 at.%; grain sizes are non-statistical values * be aware of changes in magnification ** the preparation caused numerous breakouts, which are no porosity of the samples (a) 9.1 at.% C, grain size about 300 µm (b) 11.1 at.% C, grain size about 3–70 µm (c) 13.3 at.% C, grain size about 5–60 µm (d) 18.8 at.% C, grain size about 0.1–1.5 µm.

size of the initial amorphous boron and graphite powder particles (cf. Table 1). In addition the X-ray patterns of the hot pressed samples (Fig. 9a) do show no free boron or carbon. Therefore, the diffusion of boron and carbon should be fast enough to guaranty complete solution (more than about 99 vol.% related to total specimen volume) of boron and carbon in the boron carbide within the homogeneity range of boron carbide during hot pressing at 2050 °C.

3.4. Densification during sintering

Fig. 6 shows two sintering stages. The sintering process is based on reaction controlled phase sintering in stage I between about 1300 °C and 1500 °C and solid state sintering of boron carbide in the final sintering stage II above about 1500 °C. The sintering stage I of the sandwich is extended up to about 1600 °C, because of the still available boron and carbon reservoir on top and bottom of the boron carbide layers (Fig. 4), which provides diffusion limited boron and carbon for the boron carbide reaction. State I leads to only little densification (cf. Fig. 7a). The beginning of state II between about 1500 to 1650 °C shows no densification. The main sintering based densification is observed in stage II between about 1650 and 2050 °C.

Hot pressing at 2050 °C (sintering parameters in Table 3) produces dense tablets (relative density > 99%) for all carbon contents (Fig. 7). This shows that sufficient time leads to complete densification for all investigated boron–carbon compositions. The achieved relative density corresponds with literature.[19] This makes the samples comparable with concern to thermoelectric characterisation.

3.5. Microstructure characterisation

3.5.1. FESEM

Hot pressing at 2050 °C led to a grain growth, which was significantly depending on the carbon content. At 9.1 at.% carbon content of the initial weight the largest grains are observed reaching about 300 μm (Fig. 8a). With increasing carbon content the grain growth gets less until no significant grain growth is observed at 18.8 at.% carbon (Fig. 8d). At 18.8 at.% carbon the grains reached a size between about 0.1–1.5 μm, which is in the range of the size of the initial powder particles (Table 1). Domain-like structures are observed in a large number of grains in all samples (Fig. 8).

3.5.2. X-ray diffraction and lattice parameters

The main parameter related to the specific phase formation is the boron–carbon ratio of the starting mixture. The phase analysis via X-ray diffraction of the hot pressed samples (Fig. 9a) shows clearly the reactive formed boron carbide ($B_{13}C_2$) phase. The phase analysis via X-ray diffraction is in good correspondence with the chemical analysis (Table 4). The impurities were evaporated during sintering process (thermal analysis, Fig. 3), dissolved in the boron carbide or did form phases with a not detectable volume content (less than about 1 vol.% related to total specimen volume). 8.8 at.% carbon content is the boron rich border and 18.8 at.% is the carbon rich border of the homogeneity range of boron carbide.[11] No major loss of boron or carbon appears during sintering process (cf. TG curve Fig. 3), otherwise boron reflexes should be observed at 9.1 at.% carbon content or, respectively, carbon reflexes should be observed at 18.8 at.% carbon content of the initial weight (Fig. 9a).[20–22]

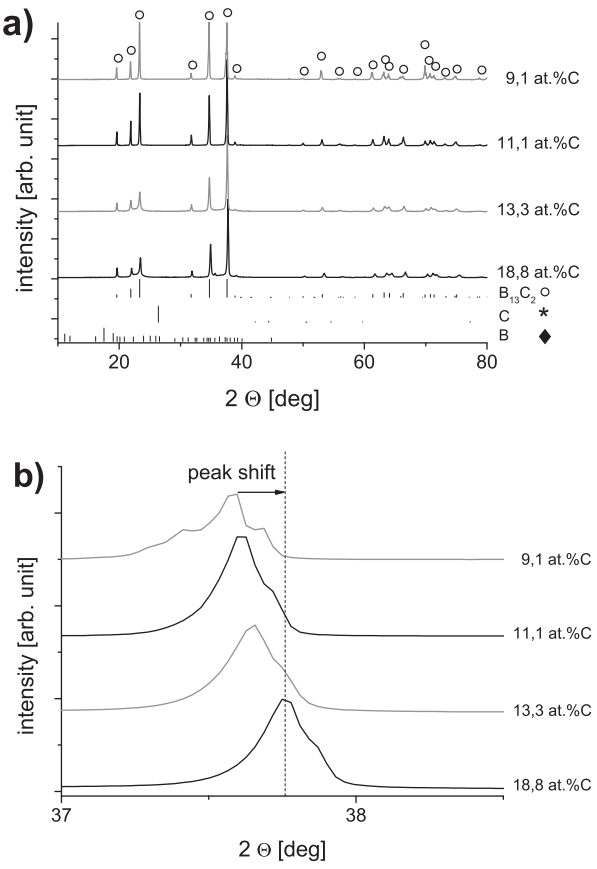

Fig. 9. Diffraction patterns of the hot pressed (2050 °C) samples in dependence of the carbon content of the initial weight (ICSD powder diffraction file numbers: boron carbide B13C2, 01-077-7011[20]; graphite C, 00-041-1487[21]; hexagonal boron B, 00-011-0618.[22]

A peak shift is observed with increasing carbon content (Fig. 9b), which is the result of the decreasing lattice parameters *a* and *c*. The calculated lattice parameters of the boron carbides (Fig. 10) show the solution of carbon into the boron carbide structure. With increasing carbon content the lattice parameter *a* decreases from 5.636 to 5.602 Å and the lattice parameter *c* decreases from 12.197 to 12.088 Å because of the smaller atomic radius of carbon compared to boron.[23–25]

Our achieved lattice parameters correspond close to the literature values of Kwei et al.,[23] Telle[24] and Aselage et al.[25]

3.6. Thermoelectric properties

The two thermoelectric properties Seebeck coefficient (S) and electrical conductivity (σ) of the hot pressed specimens with 11.1, 13.3 and 18.8 at.% carbon content of the initial weight were measured to calculate the power factor $S^2\sigma$ (Fig. 11). The Seebeck coefficient increases with increasing

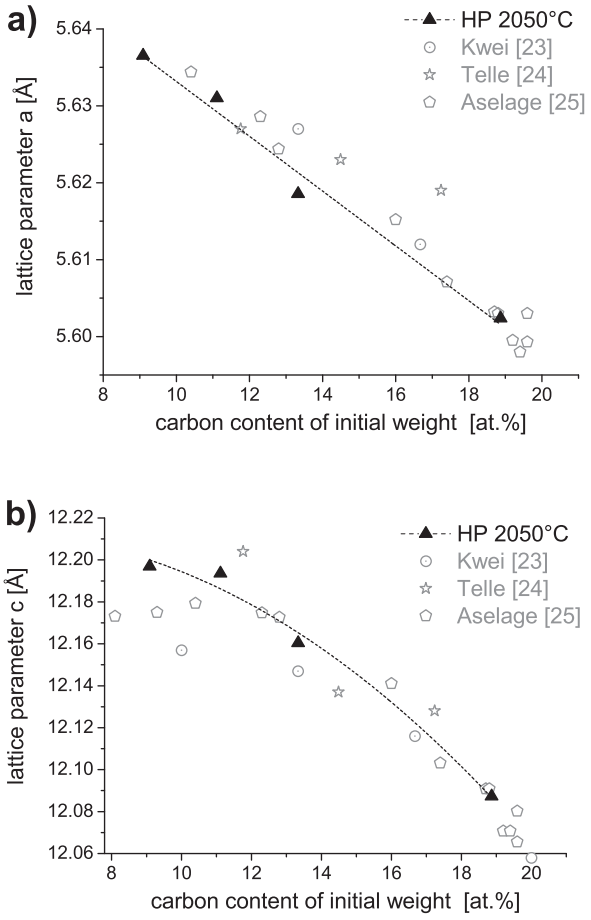

Fig. 10. Lattice parameters *a* and *c* of the hot pressed samples (HP 2050 °C) in dependence of the carbon content of the initial weight and in comparison to literature.[23–25]

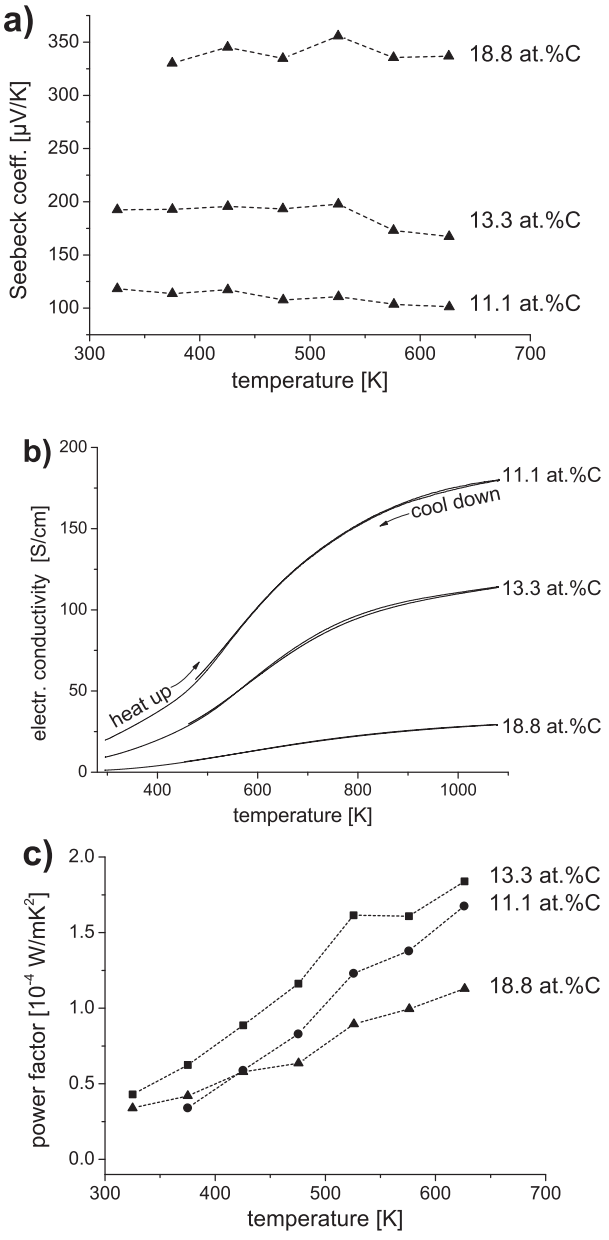

Fig. 11. Thermoelectric properties depending on temperature and carbon content of initial weight (a) Seebeck coefficient (b) electrical conductivity (c) power factor.

carbon content and shows relatively stable values in the temperature range from 325 K to 625 K at the same carbon content (Fig. 11a).

The electrical conductivity decreases with increasing carbon content and increases with increasing temperature from 300 K to 1073 K (Fig. 11b).

The heating up curves of the electrical conductivity are almost identical to the cool down curves (Fig. 11b).

The maximum electrical conductivity was obtained with sample 11.1 at.% carbon content of the initial weight at 1073 K with about 180 S/cm. Werheit et al.[3] showed comparable electrical conductivities of boron carbides in the range from about 100 to 180 S/cm at 1073 K. Low carbon content boron carbides show giant grain growth as observed by FESEM investigation of cross sections. Large grains could enhance the electrical conductivity. Furthermore the electronic state of the grain boundaries may be different to boron carbides derived from other boron carbon ratio mixtures. The slight change of crystallographic features could also contribute to the observed increase of electrical conductivity. Grain boundaries control the electrical conductivity if they form electronic barriers inside the bulk.[26,27] The change of B-C ratio within the grains could influence the level grain boundary barrier height by changing the electronic state inside the grain volume. Up to now we did not find a proof for this hypothesis. But it could be investigated in future more detailed. If there is an increase of the knowledge those findings can become a lever to design the thermoelectric properties of boron carbide.

The Seebeck coefficient increases with increasing carbon content and shows almost constant values in the temperature range from 325 K to 625 K (Fig. 11a) for the single B_xC compounds. The observed rise of the Seebeck coefficient (Fig. 11a) with increasing carbon content from 11.1 to 18.8 at.% carbon content of the initial weight is in correlation to literature.[3] Aselage et al.[28] obtained a minimum of the Seebeck coefficient at a about 13.3 at.% carbon content. Werheit[3] obtained minimum of the Seebeck coefficient at a about 12.5 at.% carbon content. The absolute value of our obtained minimal Seebeck coefficient (11.1 at.% C) of 105 µV/K is about 75 µV/K lower than that

from Aselage et al.[28] and about 105 μV/K lower than that from Werheit.[3] Our found Seebeck coefficient at 13.3 at.% carbon content with about 190 μV/K is in good correlation with Aselage et al.[28] and Werheit.[3]

The smaller grain size with more interruptions of homogeneity in boron carbide material may contribute to the increase of the Seebeck Coefficient. Additionally the change in B_xC crystallography alters the electronic state.[5] The contrary relation of Seebeck coefficient and electrical conductivity correlates to the accepted theory for bulk materials. Furthermore it is in correlation with the made hypothesis concerning the role of grain boundary barriers.

Consequently, the power factor increases with increasing temperature almost proportional to the electrical conductivity in the temperature range from 325 K to 625 K (Fig. 11c). The highest power factor was obtained at 13.3 at.% carbon content of the initial weight at 625 K with 1.84×10^{-4} W/mK^2. With a further increase of the electrical conductivity an associated increase of the obtained power factors up to 1073 K can be expected.

4. Summary and conclusions

Boron carbide ceramics were manufactured by synthesis of boron rich boron carbide from elemental boron carbon mixtures during compaction by hot pressing at 2050 °C.

Detailed investigations of the sintering process generated new insight in the mechanism of boron carbide formation and the related compaction of the ceramic material. The used methods thermal and chemical analysis, XRD and FESEM produced consistent results. The boron carbide formation occurs around 1333 °C by an instant formation of boron rich boron carbide. The performed diffusion experiment indicates high solid state diffusion of boron and carbon and no interruption of the diffusion process which could be caused by a boron carbide layer. This strong diffusion activity leads to the immediate formation of the final boron carbide which is completely finished at about 1500 °C. The FESEM investigations and the densification of the sintered ceramics indicate that an increasing boron content enhances the diffusion rate. Giant grain growth is observed particularly for the boron rich samples.

Apart from the well-known dependencies of electrical conductivity and Seebeck Coefficient to boron carbon ratio[1–3] the dimensions and structure of boron carbide grains contribute to the discussed material properties. Large boron carbide grains promote the electrical conduction but decrease the Seebeck Coefficient of the material. The change in material structure is a significant parameter to design the thermoelectric properties of boron carbide so that the manufacture technology of boron carbide materials offers a potential tool to increase the thermoelectric efficiency of boron carbide materials.

Acknowledgement

Parts of the reported work are funded by the European Union and the Free State of Saxony SAB-Grant No. 100069911 and 13923/2379.

References

1. Wood C, Emin D. Conduction mechanism in boron carbide. *Phys Rev B* 1984;**29**(8):4582–7.
2. Aselage TL, Emin D, McCready SS. Conductivities and Seebeck coefficients of boron carbides: softening bipolaron hopping. *Phys Rev B* 2001;**64**(5):0543021–8.
3. Werheit H. Thermoelectric properties of boron-rich solids and their possibilities of technical application. In: *25th Int Conf Thermoelectr*. 2006. p. 159–63.
4. Goldsmid HJ. *Introduction to thermoelectricity*. first ed. Berlin, Heidelberg: Springer; 2009.
5. Werheit H. Present knowledge of electronic properties and charge transport of icosahedral boron-rich solids. *J Phys Conf Series* 2009;**176**: 012019.
6. Schmechel R, Werheit H. On the dynamical conductivity in icosahedral boron-rich solids. *J Phys Condens Mat* 1996;**8**(39): 7263–75.
7. Balaz S, Dimov DI, Boag NM, Nelson K, Montag B, Brand JI, et al. The electronic structure of 1,2-PCB10H11 molecular films: a precursor to a novel semiconductor. *Appl Phys A* 2006;**84**:149–59.
8. Mori T, Nishimura T. Thermoelectric properties of homologous p- and n-type boron-rich borides. *J Solid State Chem* 2006;**179**: 2908–15.
9. Mori T, Nishimura T, Yamaura K, Takayama-Muromachi E. High temperature thermoelectric properties of a homologous series of n-type boron icosahedra compounds: A possible counterpart to p-type boron carbide. *J Appl Phys* 2007;**101**:0937141–4.
10. Maruyama S, Miyazaki Y, Hayashi K, Kajitani T, Mori T. Excellent p-n control in a high temperature thermoelectric boride. *Appl Phys Lett* 2012;**101**:1521011–4.
11. Schwetz KA, Karduck P. Investigations in the boron─carbon system with the aid of electron probe microanalysis. *J Less Common Met* 1991;**175**: 1–11.
12. Bouchacourt M, Thévenot F. The properties and structure of the boron carbide phase. *J Less Common Met* 1981;**82**:227–35.
13. Bouchacourt M. *Études sur la phase carbure de bore – corrélations propriétés-composition*. France: INPG, Ecole des Mines de Saint – Etienne; 1982 [doctoral thesis].
14. Thévenot F. Boron carbide – a comprehensive review. *J Eur Ceram Soc* 1990;**4**:205–25.
15. Sinha A, Mahata T, Sharma BP. Carbothermal route for preparation of boron carbide powder from boric acid–citric acid gel precursor. *J Nucl Mat* 2002;**301**:165–9.
16. Najafi A, Golestani-Fard F, Rezaie HR, Ehsani N. A novel route to obtain B_4C nano powder via sol–gel method. *Ceram Int* 2012;**38**(5): 3583–9.
17. Anselmi-Tamburini U, Munir ZA, Kodera Y, Imai T, Ohyanagi M. Influence of synthesis temperature on the defect structure of boron carbide: experimental and modeling studies. *J Am Ceram Soc* 2005;**88**(6): 1382–7.
18. Wang CB, Zhang S, Shen Q, Zhang LM. Investigation on reactive sintering process of boron carbide ceramics by XRD. *Mater Sci Technol* 2009;**25**(6):809–12.
19. Kalandadze GI, Shalamberidze SO, Peikrishvili AB. Sintering of boron and boron carbide. *J Solid State Chem* 2000;**154**:194–8.
20. Will G, Kirfel A, Gupta A, Amberger E. Electron density and bonding in $B_{13}C_2$. *J Less Common Met* 1979;**67**:19–29.
21. Tucano P, Chen R. Structure of graphite by neutron diffraction. *Nature* 1975;**258**:136.
22. Amendola A. *ICDD grant-in-aid*. New York: Polytechnic Institute of Brooklyn; 1959.
23. Kwei GH, Morosin B. Structures of the boron-rich boron carbides from neutron powder diffraction: implications for the nature of the inter-icosahedral chains. *J Phys Chem* 1996;**100**(19):8031–9.
24. Telle R. *Aufbau und Sinterverhalten mehrphasiger Keramiken im Hartstoffsystem B4C-Si*. Stuttgart, Germany: University of Stuttgart; 1985 [dissertation].

25. Aselage TL, Tissot RG. Lattice constants of boron carbides. *J Am Ceram Soc* 1992;**75**(8):2207–12.
26. Broniatowski A. Electronic states at grain boundaries. In: Harbeke G, editor. *Polycrystalline semiconductors*. Berlin, Heidelberg: Springer; 1985. p. 95–117.
27. Kondo A. Electrical conduction mechanism in recrystallized SiC. *J Ceram Soc Jpn* 1992;**100**(1166):1225–9.
28. Aselage T, Emin D, McCready SS, Duncan RV. Large enhancement of boron carbides' Seebeck coefficients through vibrational softening. *Phys Rev Lett* 1998;**81**:2316–9.